Wear 271 (2011) 640–646

Contents lists available at ScienceDirect

Wear

journal homepage: www.elsevier.com/locate/wear

Enhanced wear resistance in $AlMgB_{14}$–TiB_2 composites

B.A. Cook[a,*], J.S. Peters[a], J.L. Harringa[a], A.M. Russell[a,b]

[a] Ames Laboratory, Division of Materials Science & Engineering, Iowa State University, Ames, IA 50011, United States
[b] Department of Materials Science & Engineering, Iowa State University, Ames, IA 50011, United States

ARTICLE INFO

Article history:
Received 31 August 2010
Received in revised form
19 November 2010
Accepted 21 November 2010
Available online 15 April 2011

Keywords:
Mechanical alloying
Ceramic matrix composites
Erosive wear
Abrasive wear
Borides

ABSTRACT

Studies of bulk $AlMgB_{14}$ and TiB_2 composites have shown that these materials exhibit exceptional resistance to erosive and abrasive wear. Multi-hour ASTM erosion tests with Al_2O_3 abrasive against composite samples comprised of $AlMgB_{14}$ (40 vol.%) and TiB_2 (60 vol.%) resulted in erosion rates of 0.5 mm^3/kg of erodent, compared with 10.5 mm^3/kg for wear-resistant grades of WC–6% Co. Increasing the TiB_2 fraction to 80 vol.% further reduced erosion rates to as low as 0.26 mm^3/kg. Fracture nucleation in the TiB_2 grains was identified by SEM analysis as a primary damage mechanism. Additionally, diamond abrasion testing revealed a slightly different trend between composition and wear than that observed in erosion testing. Results of wear tests are discussed in terms of microstructure, hardness and indentation toughness of each phase, and grain boundary cohesion. Analysis suggests several energy dissipative mechanisms including fracture termination at grain boundaries and conversion of mechanical energy to thermal energy act to improve wear resistance in the fine-grained boride composites.

1. Introduction

Material degradation by wear increases operating costs, decreases productivity, and reduces energy efficiency across a broad range of applications [1,2]. Operations and devices such as mining, petrochemical processing, machining and metal forming, abrasive fluid transport, and microelectromechanical systems will require improved materials in order to increase efficiency and overcome performance limitations imposed by conventional materials. The search for new materials possessing increased resistance to wear spans the entire spectrum of materials ranging from metallic [3–7] to ceramic [8–11] to advanced composites [12–16]. Erosive wear may be viewed as mechanical or physical surface damage resulting from impingement by solid particles or liquid droplets. It is a function of the number of impacts and the momentum transferred per impact. Erosion is typically measured by the change in mass (or volume) of a material after exposure to an abrasive particle flux. Variables include impingement angle, particle speed upon impact, particle morphology, and duration of erosion. As discussed by Finnie and Natesan [17], erosive wear typically reaches a maximum in metallic systems at a glancing impact angle of 30°, whereas maximum erosion in ceramic-based materials occurs at normal (90°) impact. Some studies of cemented carbides indicate brittle fracture with maximum erosion occurring near 90° [18]. Other studies of steady-state erosion in cemented carbides found a maximum erosion corresponding to an impingement angle of about 70°, intermediate between pure ductile and brittle behavior [19]. As discussed by Hovis et al. [20], the damage mechanisms depend on the ratio of erodent size to grain size, wherein brittle failure is associated with smaller values of this ratio and ductile failure with larger values. Several studies have focused exclusively on the wear resistance of composite materials, from both an experimental [21,13,22,23] and theoretical [24] perspective.

Recently, a new class of ceramic matrix–ceramic reinforcement composites has been developed, exhibiting microhardness values as high as 35–40 GPa [25,26]. These composites have shown potential as cutting tools [27,28] and also as wear-resistant, low-friction protective coatings [29,30]. The purpose of this study was to evaluate the potential for these composites as wear-resistant articles in severe erosive and abrasive environments.

2. Experimental details

In the present work, samples for erosion testing were synthesized by hot pressing submicron powders produced by mechanical alloying (MA) of the elemental constituents. Stoichiometric quantities of high-purity Al wire (Cominco) and distilled Mg strands (United Minerals & Chemicals, Inc.) were added to vacuum-outgassed amorphous B powder (SB Boron Corp.) high-purity argon and subsequently blended with 60 volume percent TiB_2. Samples prepared with TiB_2 obtained from the MA of elemental −325 mesh Ti (Aesar) and amorphous B obtained a fine, submicron microstruc-

* Corresponding author at: 221 Metals Development, Materials & Engineering Physics Program, Ames Laboratory, Iowa State University, Ames, IA 50011-3020, United States. Tel.: +1 515 294 9673; fax: +1 515 294 8727.
E-mail address: cook@ameslab.gov (B.A. Cook).

0043-1648/$ – see front matter © 2011 Published by Elsevier B.V.
doi:10.1016/j.wear.2010.11.013

Table 1
Composition, density, hardness, major impurity or secondary phases, and erosion rate of selected materials examined in this study.

Composition	TiB_2	Density (%)	Hardness (GPa)[a]	Impurity or secondary phases	Erosion rate (mm^3/kg)[b]
$AlMgB_{14}$–60 vol.% TiB_2[c]	MA	96.1	35	$MgAl_2O_4$, FeB	0.49
$AlMgB_{14}$–60 vol.% TiB_2[c]	MM	96.1	32	$MgAl_2O_4$, FeB	0.59
$AlMgB_{14}$–80 vol.% TiB_2[c]	MM	97.1	30 (5 kg)	$MgAl_2O_4$, FeB	0.26
100% TiB_2[c]	MM	98.7	30	Ti(C,N)	0.75
WC–6 wt.% Co	–	~100	17	Co, Ta	10.5

[a] Vickers microhardness values were determined with a 1 kg load except where otherwise indicated.
[b] Erosion testing performed with 200 μm Al_2O_3 grit at 77 m/s and 4.5 g/min.
[c] All prepared samples consolidated by hot pressing for 60 min at 1400 °C under 105 MPa pressure.

ture, with an average grain size ranging from 200 to 800 nm. By contrast, samples produced from mechanical milling (MM) of commercial TiB_2 powder (Aesear −325 mesh) were found to possess a relatively coarse microstructure, with a wide distribution of grain sizes, ranging from slightly less than 1 μm to as large as 10 μm in heavily agglomerated regions. Samples prepared with mechanically alloyed TiB_2 or commercial TiB_2 are hereafter referred to as MA or MM composites, respectively. All samples were consolidated by hot pressing under flowing argon in a BN-coated graphite die at 1400 °C for 60 min under an applied pressure of 105 MPa. The above samples were prepared in order to compare the effect of processing and the resultant microstructure on wear resistance. Another set of samples was prepared by the same methods except by varying the concentration of TiB_2 from 30 to 100 vol.%. All of these samples were prepared with MM TiB_2 for ease of processing. A fine-grained, wear resistant WC–6% Co tooling insert was also evaluated for comparison (Kennametal, K-68®). Selected compacts were metallographically mounted, polished, and characterized for microstructure using a JEOL JSM-5900 SEM. Density was measured by Archimedes' displacement method.

Erosive wear was measured by subjecting samples to 90° impact from angular Al_2O_3 abrasive entrained in a regulated gas stream at a distance of 1 cm from the end of the nozzle. Abrasive impact speed was fixed at 77 m/s, as determined by high-speed digital photography. Erosion was interrupted for measurement of sample mass at hourly intervals for a total test time of 4 h. Precise positioning of the sample in a specially designed holder ensured that all erosion occurred in the same crater. The samples were subjected to erosion by 200 μm Al_2O_3 at a nominal mass flow rate of 4.5 g/min. Samples were ultrasonically cleaned in ethanol and thoroughly dried prior to the start of erosion testing, and again before each incremental mass measurement. To minimize effects from solvent absorption samples were weighed only after a specified drying time of 15 min including the same wash/dry treatment for the initial measurement before erosion testing. Ten or more mass readings were taken on each specimen, and the results were averaged to obtain accuracy within 0.1 mg. The Al_2O_3 abrasive was collected after impact and not reused. Selected samples were also subjected to brief exposure to a 100-μm Al_2O_3 flux at a 45° impingement angle at a higher velocity of 200 m/s using a commercial grit blast system in order to accelerate initiation of fracture and thermal effects during the initial stages of erosion. Erosion rates, E_r, were calculated from Eq. (1),

$$E_r = \frac{\Delta m}{t} \times \frac{1}{\Phi} \times \frac{1}{\rho} \quad (1)$$

where Δm is the mass loss resulting from erosion during a time t, Φ is the erodent mass flow rate, and ρ is the density of the sample.

Abrasion testing was performed by positioning a flat surface of each sample against a lubricated diamond belt under a fixed load of 6.7, 13, or 22 N. Using electro-discharge machining (EDM), an edge was sectioned on each sample resulting in a flat, 9 mm × 3 mm face. The faces were polished with 45 μm diamond grit to remove the texture from EDM and ensure a similar initial finish for all samples. The samples were positioned face-down against a belt bonded with 400 grit (23 μm) diamond. The belt was constantly lubricated with water while operated at linear speeds ranging from 0.5 to 2.0 m/s. Because wear of the belt and abrasive is unavoidable with a fixed abrasive system, the abrasive belt track was used only once for each test. In other words, each sample was repositioned horizontally across the abrasive belt before starting a test, to create a new wear track on an unused portion of the belt. The sample holder was designed to hold a mass of the weights listed above, resulting in contact pressures of 250–820 kPa. The samples were tested for 2 min at each testing condition. Abrasive wear was measured by mass loss; each sample was cleaned and weighed as described above for erosion testing.

3. Results and discussion

Table 1 lists various properties of composite samples with MA or MM TiB_2 compared to the commercial WC standard. Hardness and indentation toughness in these composites is a function of $AlMgB_{14}$:TiB_2 ratio, grain size, porosity, and impurity content, which in previous research reached a maximum in the 50–60 vol.% TiB_2 composition range; the effects of varying the ratio of $AlMgB_{14}$ to TiB_2 on microhardness and abrasion resistance have been discussed in a previous publication [31]. Microstructure has been found to be a critical parameter in determining hardness, toughness, and wear resistance [32]. All of the hot-pressed boride composites contain from 2 to 4 vol.% porosity, as determined by Archimedes density and SEM microscopy. Porosity decreases hardness and wear resistance, as demonstrated previously in liquid-phase sintered alumina [33]. Agglomeration of the dry powders results in non-uniform microstructures and a concomitant reduction in hardness.

X-ray diffraction patterns of $AlMgB_{14}$–TiB_2 composites indicate that $MgAl_2O_4$ spinel and iron boride are the major impurities [34]. Neutron activation and inductively coupled plasma mass spectrometry revealed up to 5 vol.% oxygen and 10 vol.% iron phases. Iron is introduced during mechanical alloying from wear debris of the hardened steel media and vial liner. The major source of oxygen is believed to be surface contamination of the precursor powders. A small amount of iron contamination is actually beneficial because it acts as a sintering aid, increasing densification of the boride. However, larger amounts of iron have a deleterious effect on hardness and wear resistance. The FeB and $MgAl_2O_4$ phases are undesirable because of their lower hardness and fracture toughness vis-à-vis the $AlMgB_{14}$ and TiB_2 phases.

3.1. Erosion

Results of steady-state erosion tests are shown graphically in Fig. 1, which presents cumulative volume loss as a function of time for two $AlMgB_{14}$–60 vol.% TiB_2 composites and also the fine-grained WC–6 wt% Co insert. The boride composites' steady-state erosion

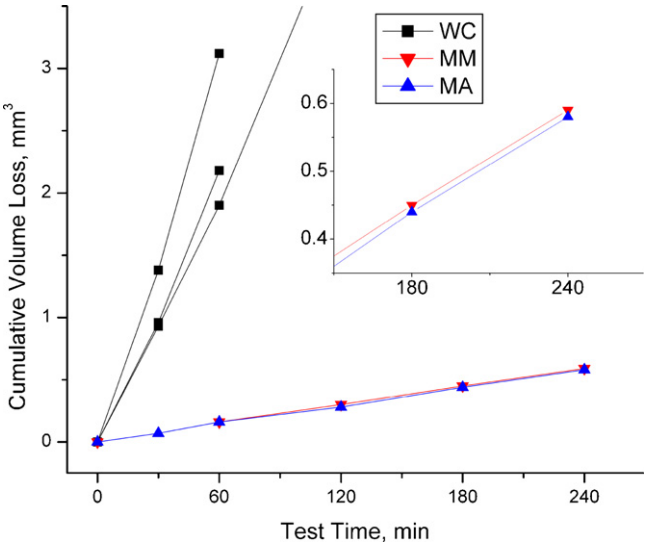

Fig. 1. Steady-state erosion behavior of fine-grained WC–6 wt.% Co and two samples of $AlMgB_{14}$–70 wt.% TiB_2. Erosion conditions: 200 μm Al_2O_3, 77 m/s particle velocity; 1 cm standoff distance; 4.5 g/min mass flow rate; 90° impingement angle.

wear rates were 15–20 times lower than the WC–Co erosion rates. The erosion rate of the boride composites ranged from 0.49 mm^3/kg to 0.59 mm^3/kg, in contrast to 10.5 mm^3/kg for the erosion rate of the carbide insert.

Data from erosion testing was assumed to be taken within the steady-state regime. Any effect from an incubation period during the first hour of testing was indistinguishable from the statistical error of subsequent testing and thus presumed to be minimal. In support of this justification, erosion craters were fully formed before 30 min of testing and qualitative SEM observation revealed erodent adhesion/removal rates to be at steady state. The effect of erodent adhesion on mass measurements during the incubation period was also presumed to be below detection limits as no more that 5–10% of the erosion surface was covered by adhered erodent at any given time; additionally adhered material was very thin and comprised only a small fraction of each erodent particle's original mass. Any incubation period was not directly measured during testing (presumed to be on the order of minutes) due to the testing set-up and the low mass changes that would be expected during such brief testing.

During erosion of WC, the ductile Co binder is compromised by plastic deformation, resulting in unsupported WC grains that fracture and lead to grain ejection. The intersection of fracture surfaces during erosion leads to rapid material removal and grain pullout as seen in Fig. 2. Identical conditions imposed on an $AlMgB_{14}$–TiB_2 composite reveals evidence of incipient fracture in the (lighter contrast) TiB_2 phase. The erosion of brittle materials typically proceeds by repeated fracture from particle impacts followed by the ejection of chips that form as the microcracks coalesce. In the case of the $AlMgB_{14}$–TiB_2 composite, extensive, well-developed cracks are not observed. Examination of samples subjected to higher velocity erosion revealed that the incipient cracks propagate to the TiB_2 grain boundaries and subsequently terminate. This observation suggests that the primary phase responsible for damage initiation is TiB_2, and an example of a nascent fracture in this component is shown in Fig. 3. In the figure, the arrows indicate nucleation sites for microfracture occurring within the TiB_2 phase (light contrast region), which are seen to terminate at the interface between that phase and the $AlMgB_{14}$. In Fig. 4, progression of cracks such as those in Fig. 3 lead to TiB_2 grains larger than 1 μm fracturing internally. Failure does not occur at the $AlMgB_{14}$–TiB_2 grain boundary, despite the damage within the large grains, again demonstrating the strong bonding between the phases. The observed fracture and grain pullout of TiB_2 suggests reduction of the TiB_2 particle size as a viable path to improved toughness and wear resistance.

A number of empirical relationships describing erosion have been advanced over the years. In particular, Lawn's approach [35] relating indentation toughness, K_{1c}, and hardness, H, to erosive wear volume lost per impact, V, in a perfectly brittle material, is

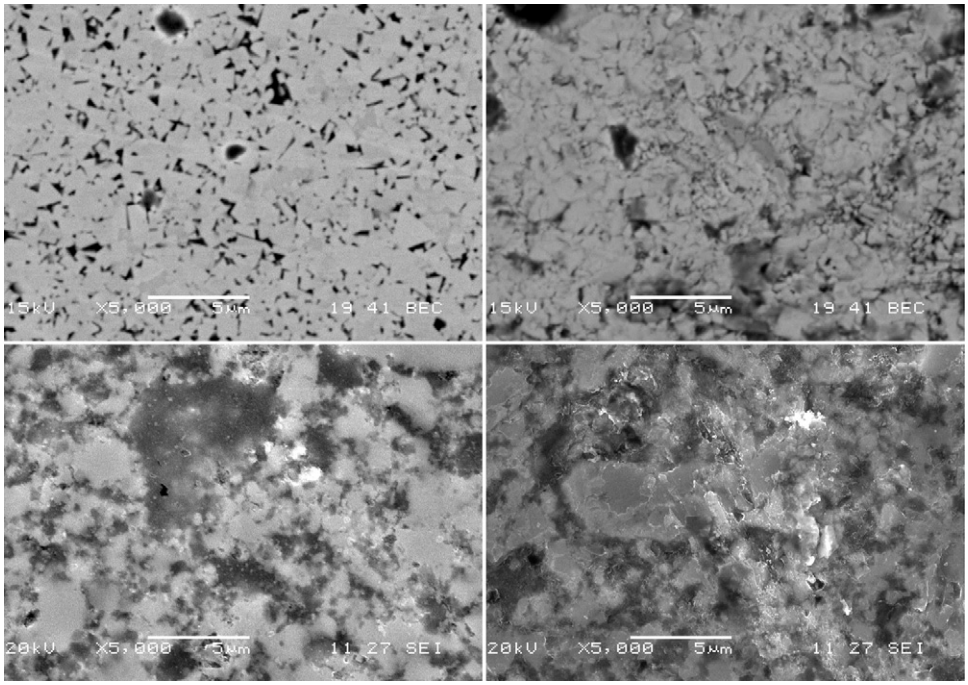

Fig. 2. (Top) SEM micrograph of as-polished WC–6%Co insert before erosion (left) and after 5 s of erosion at an erodent velocity of 200 m/s (right). (The WC grains appear light while the Co binder appears dark in the as-polished micrograph.) Note the fracture within and between individual WC grains, leaving numerous regions devoid of material. (Bottom) Corresponding views of the $AlMgB_{14}$–70% TiB_2 before and after erosion under identical conditions.

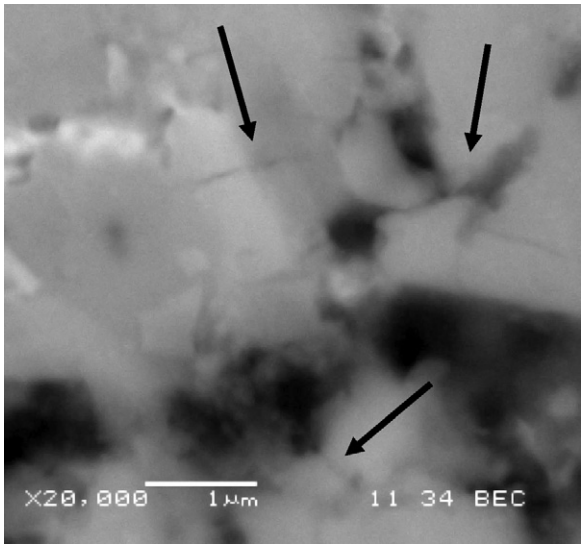

Fig. 3. Micrograph showing fracture nucleation in $AlMgB_{14}$–TiB_2 after 5 s of exposure to high velocity (200 m/s) erosive grit. Arrows indicate position of microcracks both within and between the TiB_2 grains.

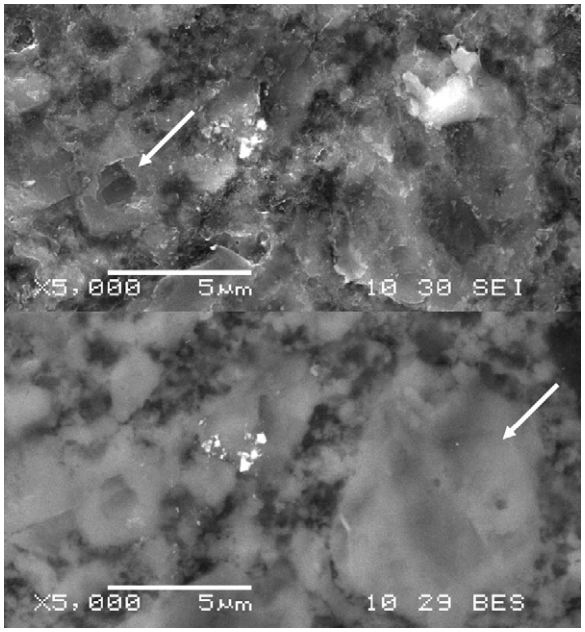

Fig. 4. Topographical (top) and compositional (bottom) micrographs of MM 60 vol.% TiB_2 sample after erosion. Arrows indicate failure entirely within larger TiB_2 grains. 4 h erosion at 77 m/s.

described by Eq. (2)

$$V = \frac{\omega P_i^{11/16}}{K_{1c}^{4/3} H^{1/2}} \quad (2)$$

where ω is a wear coefficient and P the impulsive load. Consequently, in a perfectly brittle solid, fracture toughness is expected to contribute more strongly to erosive wear resistance than hardness. In a complex, multiphase material such as the $AlMgB_{14}$–TiB_2 composites, the generation of lateral impact cracks may require more energy than in a single-phase material. Moreover, other energy dissipating mechanisms may contribute to increased resistance to wear, as discussed below.

Eq. (2) was developed based on studies of glass, an amorphous material with no microstructure dependence and thus no scale dependence [35]. Other studies by Lawn discuss microstructure and scale dependence; for example, glass–ceramic composites of different reinforcement size exhibit toughness increasing with grain size while strength decreases [36]. Additionally, he explains that toughness is lower for short crack lengths where intrinsic properties (i.e. material or grain boundary strength) dominate over microstructure-dependent toughening mechanisms. This may help to explain the differences in erosion behavior between the WC–Co and $AlMgB_{14}$–TiB_2 composites. At scales on the order of the grain size of the materials, the intrinsic material properties become dominant; as shown in Figs. 2 and 3 crack lengths are typically on the order of 1 μm. In the case of the cermet, the WC phase exhibits brittle failure while the Co phase provides little structural reinforcement due to its low hardness. In the boride composite, both phases are hard and possess lower toughness than the WC cermet, yet the short cracks are deflected quickly due to the highly refined microstructure. This is an energy absorbing mechanism that increases toughness at small scales during erosion, but is not observed at larger scales. Thus WC–Co and $AlMgB_{14}$–TiB_2 exhibit opposite trends in toughness with respect to scale. Toughness itself depends on the measurement conditions, and the scale at which these measurements are valid can be dependent on microstructure. Toughness estimated by the Palmqvist technique may be a poor indicator of energy absorption during erosive impact, making wear performance difficult to predict based on Eq. (2) alone. It is possible that the fine microstructure of the boride composites encourages energy absorption mechanisms that are not seen or measured at larger scales. The deflection of cracks at low penetration depth causes material to spall from the sample in thin flakes, absorbing energy through the generation of numerous surfaces. By contrast, deeply penetrating cracks join laterally deeper in the sample, causing larger volume removal per unit of surface area generated. This is seen in both the WC–Co sample and the largest grains within the $AlMgB_{14}$–TiB_2 composite (Fig. 4).

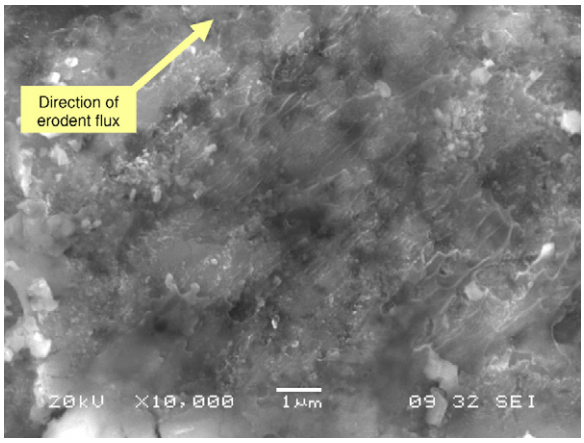

Fig. 5. High magnification image of boride composite after 125 s of cumulative erosion at 45° impingement angle and 200 m/s particle velocity. (Note evidence of material flow in the direction indicated by the arrow.)

A high-magnification SEM image of a boride composite after 125 s of high-velocity (200 m/s) erosion at a 45° angle to the surface is shown in Fig. 5, which appears to display evidence of flow of material at the surface. The direction of flow, indicated by the arrow in the figure, corresponds to the transverse component of the incident velocity vector of the erodent particles and gas. The primary oxidation product of $AlMgB_{14}$ is boron oxide, B_2O_3, which melts at a temperature of 450 °C. In order to estimate if the impacting alumina particles might generate sufficient local heating to melt boron oxide, a calculation was performed in which a particle impact was modeled as an indentation, with the energy of plastic deformation

assumed to be entirely converted into heat. An expression of the form

$$fP\delta z = mc\ \Delta T \quad (3)$$

was employed for the estimation of temperature effects, where P is the impact load, δz is the penetration depth, m is the particle mass, c is the heat capacity, ΔT is the local temperature increase, and f is the fraction of indentation energy dissipated within the plastic zone. In this approximation, f is assumed to be 0.4 (40%). The plastic zone radius is taken as 20 μm. This model predicts a temperature increase on the order of 300–700 °C within the local plastic deformation region. In agreement with this model, a faint glow can be observed during erosion testing, which indicates a surface temperature of at least 500 °C. Other studies have reported similar temperature effects, including localized melting of a glass phase [37–39]. It is known that WC exhibits rapid oxidation above 600 °C [40,41]. Our studies to 1000 °C in air have shown qualitatively that $AlMgB_{14}$ forms a glassy scale, in contrast to the catastrophic oxidation normally associated with WC.

3.2. Processing effects

Another variable that strongly affects erosive and abrasive erosion rates is the processing of the TiB_2. The MA sample was prepared with 100–200-nm mechanically alloyed TiB_2, whereas comparatively coarse commercial TiB_2 powder was blended with the $AlMgB_{14}$ powder in the MM sample. The TiB_2 was dry-mixed in each case with the $AlMgB_{14}$ powder prior to consolidation, and even though some powder agglomeration occurred in both cases during processing, the average particle size of the TiB_2 in the MA sample was considerably smaller than that in the MM sample, e.g., 200–300 nm in the MA case compared with 750–5000 nm for the MM powder, based on SEM observation. A strong interface between boride phases acts as a reinforcement, increasing both hardness and toughness [42]. For grain sizes on the order of 1 μm or larger, the response of the composite approaches a rule-of-mixtures behavior, whereas a positive deviation is observed in the case of the more highly refined microstructures. Introduction of indentation cracks on and near interfaces between $AlMgB_{14}$ and TiB_2 phases has revealed no indication of delamination or a tendency for the cracks to revert to an intergranular mode from transgranular propagation. The bond strength between $AlMgB_{14}$ and TiB_2 may be enhanced for certain favorable orientation relationships. For example, molecular orbital calculations of the interfacial energy between Al and SiC for various orientations have shown that their bonding strength can exceed the adhesive strength of pure Al [43].

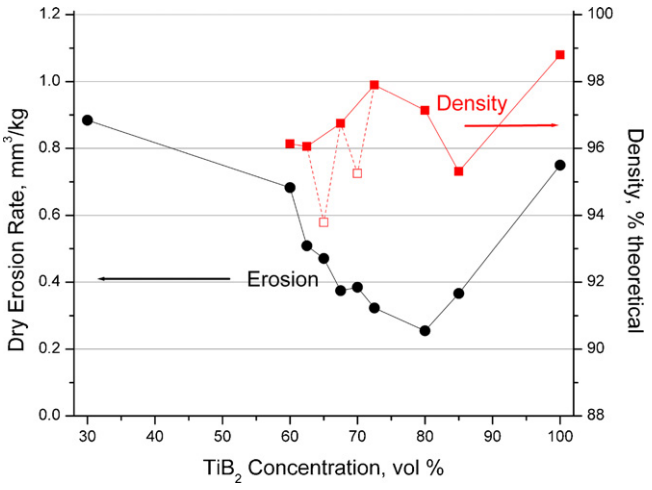

Fig. 6. Dry erosion rate for $AlMgB_{14}$–MM TiB_2 samples of various compositions. Open symbols correspond to data points for lower density samples which correspond to slight relative increases in erosion rate. Erosion conditions: 200 μm Al_2O_3, 77 m/s particle velocity; 1 cm standoff distance; 4.5 g/min mass flow rate; 90° impingement angle.

The evidence suggests that the interface between $AlMgB_{14}$ and TiB_2 may provide a critical mechanism for enhanced resistance to wear.

For a fixed abrasive particle size and kinetic energy, a relatively coarse microstructure is more likely to experience transgranular fracture, with much of the crack energy dissipated within the grains. As the grain size becomes progressively smaller, there exists less volume for transgranular fracture, and more of the crack energy will be dissipated in the interfacial boundaries between phases. But strong interfacial energy between these boride compositions makes it more likely that the crack propagation energy can be dissipated without breaking the bonds, thereby preserving the integrity of the interface. If the single-phase regions in these composites constitute the weakest link with respect to erosion resistance, then increasing the volume fraction of boride interfaces would contribute to an enhancement in wear resistance. In other words, wear resistance in these unique composites can be enhanced by reducing the occurrence of intergranular fracture through a reduction in grain size to the nanometer scale, thus constraining cracks within the grains and preventing or impeding extensive intergranular propagation, assuming the deleterious effects of oxygen can be controlled.

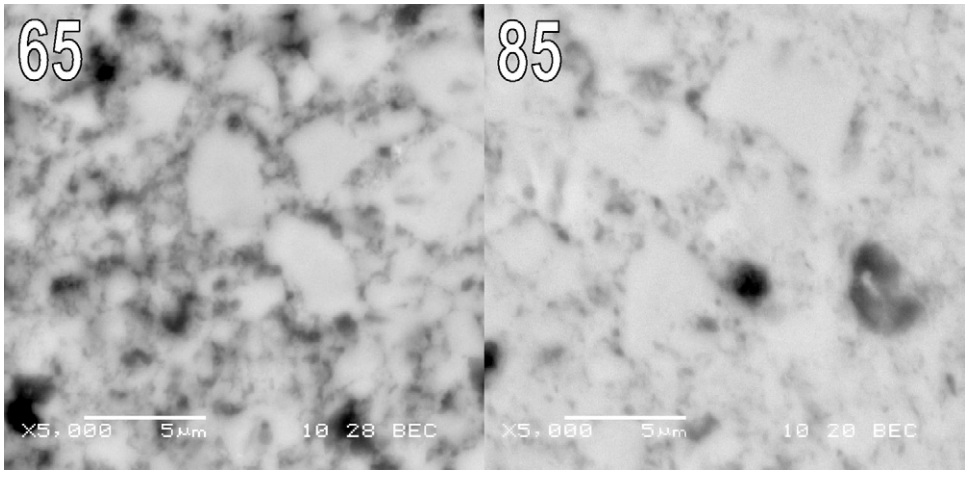

Fig. 7. Compositional micrographs of polished 65 (left) and 85 (right) vol.% TiB_2 composites showing relative morphologies of the TiB_2 (bright) and $AlMgB_{14}$ (dark) phases.

3.3. Compositional effects

Additional samples were prepared with TiB_2 concentrations spanning the range from 30 vol.% to 100 vol.%. Despite the well-documented difficulty in consolidating pure TiB_2, the sample was quite dense (98.8%) due largely to the fine grain size and low-oxygen processing as described in a previous paper [44]. Fig. 6 shows the measured dry erosion rates for these samples.

It can be seen from Fig. 6 that the erosion rate tends to decrease with increasing TiB_2 concentration, up to a maximum of 80 vol.%. TiB_2 is a highly wear-resistant phase, though its densification is difficult, resulting in porosity that is detrimental to wear resistance [33]. The 1400 °C consolidation temperature is lower than the temperatures typically employed during sintering of TiB_2 composites; with the $AlMgB_{14}$ phase possibly acting as a sintering aid. It is interesting to note the relatively high density measured in the 100% TiB_2 sample. Though prepared by the same methods and with the same starting material, the 100% TiB_2 sample contains lower O and Fe impurities due to the absence of the $AlMgB_{14}$ phase; additionally, it appears to have densified by different sintering mechanisms involving C and N, as described previously [44]. This may partially explain the higher relative density and provides insight into the mechanisms responsible for the increase in wear rate above 80 vol.% TiB_2. As described in the previous TiB_2 study, varying degrees of intergranular fracture were found [44]. To summarize, C- and N-rich impurities were found to segregate to the grain boundaries. Additionally, high concentrations of these impurities were associated with higher instances of intergranular fracture indicating weak grain boundaries. It should be noted that TiC and TiN are common additives/sintering aids for TiB_2 [45–47]. By contrast, $AlMgB_{14}$ appears to exhibit exceptionally strong bonding with the TiB_2 phase [42]. Thus, in specimens containing up to 80 vol.% TiB_2, there is an increase in erosion resistance as TiB_2 content increases due to the inherent high hardness of TiB_2 without the detrimental effect of softer and/or more poorly bonding sintering aids. High density is critical to high wear resistance; yet if sintering aids used are significantly lower in hardness or toughness, there will be a trade off between increasing the fraction of sintering aid added to remove a diminishing fraction of porosity. In the case of $AlMgB_{14}$, the intrinsic hardness is near that of TiB_2 while toughness is enhanced, relative to more poorly bonding TiC or TiN for instance, by minimizing inclusion of weak grain boundaries.

Above 80 vol.% TiB_2, the increase in erosion rate is likely due to a combination of higher porosity (due to insufficient sintering aid) and higher fraction of TiB_2–TiB_2 grain boundaries. This latter condition is likely significant, because the 100% TiB_2 sample exhibits the highest density yet its erosion rate was three times that of the 80 vol.% sample. Fig. 7 compares 65 and 85 vol.% TiB_2 sample microstructures, as the subtle changes in morphology are more distinctive. Due to the different milling characteristics of the two phases, $AlMgB_{14}$ tends to surround the TiB_2 grains, effectively separating them even at fractions of TiB_2 as high as 80 vol.%. Above this, as seen in Fig. 7, there is a higher instance of direct TiB_2–TiB_2 grain contact and the $AlMgB_{14}$ phase has become segregated to discreet particles, as opposed to a continuous matrix as in the left of the figure.

TiB_2–TiB_2 grain boundaries are susceptible to contamination from weakly bonded impurities. For example, the $AlMgB_{14}$–TiB_2 composites typically exhibit less grain boundary failure than in the 100% TiB_2 sample described above [42,44]. It is possible that the $AlMgB_{14}$ phase has a "gettering" effect with TiB_2, incorporating C and N impurities into its complex structure. Improvements in processing and mixing of the two phases could produce a coating of $AlMgB_{14}$ around each TiB_2 grain, avoiding direct TiB_2–TiB_2 contact and producing potentially stronger grain boundaries. This in turn could increase the maximum erosion resistance towards higher TiB_2 fractions by minimizing the $AlMgB_{14}$ additive necessary to both achieve proper density and to minimize TiB_2 boundary impurities.

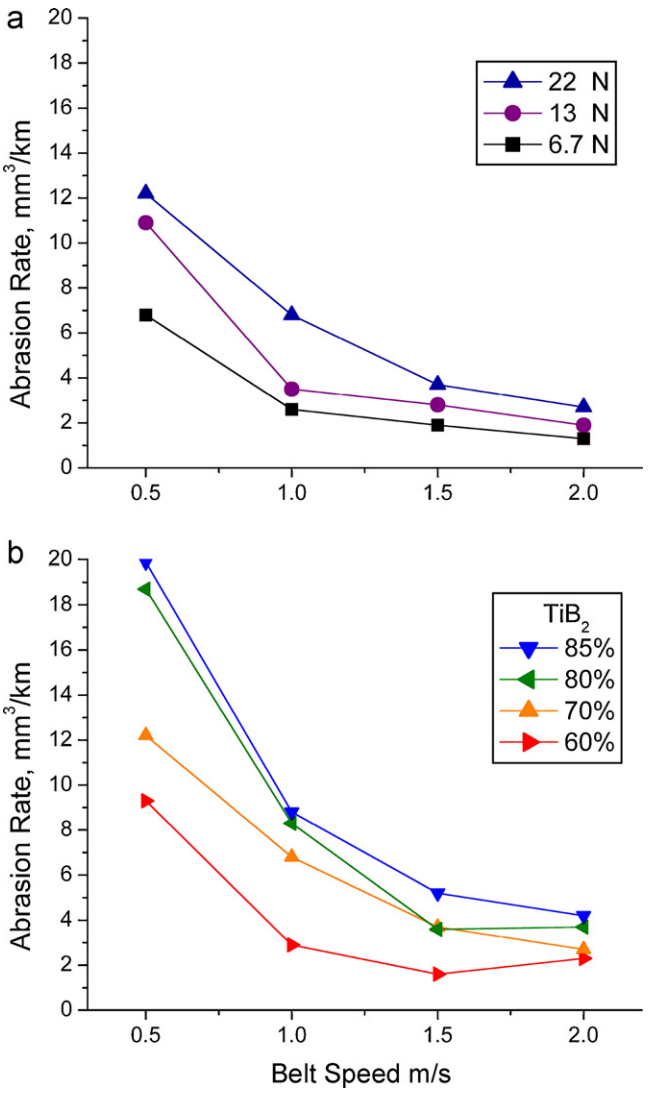

Fig. 8. (a) Diamond abrasion data for a 70 vol.% TiB_2 composite, showing typical behavior with respect to testing load and belt speed. (b) Diamond abrasion rates for selected compositions under a 22 N load at various speeds. (Note: the minimum abrasion rate measured for WC–6% Co was 27.3 mm^3/km at a belt speed of 1.5 m/s and a load of 6.7 N.).

3.4. Abrasion

Fig. 8(a) shows the measured abrasion rates of an $AlMgB_{14}$–70 vol.% TiB_2 composite as a function of belt speed and load. It is seen that the abrasion rate for this composite decreases with increasing belt speed and with decreasing applied load. As discussed above, the dry erosion rate was lowest for the 80 vol.% TiB_2 composite. Shown in Fig. 8(b) are diamond abrasion data measured at a load of 22 N, where the distinction between compositions is most apparent. Here the minimum abrasive wear rate is corresponds to the lowest TiB_2 concentration tested, 60 vol.%. In this study, abrasion was performed in water, which introduces an additional variable to the wear response of $AlMgB_{14}$–TiB_2 composites. In other studies, it has been shown that the boride composite and its associated thin films exhibit exceptionally low friction coefficients when measured in the presence of moisture [48]. This is due to the formation of boric

acid on the sample surface. Boric acid has a layered structure with weak bonding much like graphite. According to recent studies, TiB_2 is the stronger boric acid former of the two phases [48]. If the dissolution rate of boric acid is sufficiently high, this may result in a higher rate of abrasion of the higher TiB_2 concentrations.

Additionally, Fig. 8(b) shows that abrasion rate decreases with increasing belt speed. This is likely an artifact of the testing method. As stated in the procedure, each abrasion test was run for the same time; thus higher speed testing equates to longer sliding distances. Although care was taken not to re-use any portion of the belt for subsequent runs, it is very possible that belt wear during the test is significant enough to affect the results. As the materials tested were of high hardness, the initially sharp diamond abrasive tends to dull quickly and the abrasive power drops significantly, even if the belt is not yet noticeably worn. This effect is commonly experienced during routine polishing of these composites. Thus, regardless of belt speed, each sample tested experiences an initial high wear rate; the mass loss is only measured at the end of each test and for higher speed tests is also averaged over a longer distance. This testing method could be improved to more accurately describe the actual abrasive mechanisms, for instance a three-body abrasion set-up where unused diamond slurry is continuously applied to the wear surfaces. Fixed-distance instead of fixed-time testing could also help, although in this instance, if the initial "conditioning" of the abrasive belt is sufficiently rapid, it would not help to separate the effects of belt conditioning from the effects of belt speed. Still, this method is sufficient as a relative comparison of material performance even if it cannot be used to elucidate the abrasion mechanics within.

4. Conclusion

The wear resistance of $AlMgB_{14}$–TiB_2 composites and of fine-grained WC–6% Co was determined in a series of ASTM dry erosion tests employing 200-μm alumina at an impact speed of 77 m/s. The steady-state erosion rate of the boride composites was found to exceed that of the wear-resistant carbide by a factor of 15–20, depending on erodent impact speed, size, and mass flow rate. Microstructural refinement in the boride composites was found to improve erosion resistance. Analysis suggests that energy dissipative mechanisms including fracture termination at grain boundaries and conversion of mechanical energy to thermal energy act to improve wear resistance in the fine-grained boride composites. Micrographs of pristine and eroded surfaces indicate that large TiB_2 grains and TiB_2–TiB_2 grain boundaries are to be avoided as they initiate larger scale fracture that reduces overall energy absorption. The difference between the abrasion and the erosion results show how application and environment can favor different materials, even compositions. $AlMgB_{14}$, depending on application, can be used as an additive to TiB_2 primarily as a reinforcement or a sintering aid, or perhaps to tune between abrasive and erosive performance.

Acknowledgements

The authors wish to express their appreciation to Eric Ostrander and Lindsay Brown at Iowa State University for sample preparation and testing. The Ames Laboratory is operated for the U. S. Department of Energy by Iowa State University under contract DE-AC02-07CH11358. This project was supported by the Office of Industrial Technology, Office of Energy Efficiency and Renewable Energy, monitored by Dr. Mahesh Jha.

References

[1] M. Hadfield, C. Ciantar (Eds.), Proceedings of the First International Conference on Tribology in Environmental Design, Bournemouth, September 2000, PEP Publications, Chapell Hill, NC, USA, 2001, pp. 3–118.
[2] R. Chattopadhyay, Surface Wear: Analysis, Treatment, Prevention, vols. xi–xii, ASM International, Materials Park, OH, USA, 2001, pp. 267–290.
[3] M. Roy, J. Phys. D: Appl. Phys. 39 (2006) R101–R124.
[4] K. Yildizli, M.B. Karamis, F. Nair, Wear 261 (5–6) (2006) 622–633.
[5] S.G. Sapate, A.V. Rao, Wear 256 (7–8) (2004) 774–786.
[6] D. Zasada, Z. Bojar, R. Jasionowski, Archiwum Odlewnictwa 5 (18 Pt. 2) (2006) 349–356.
[7] S. Das, D.P. Mondal, S. Sawla, Metall. Mater. Trans. A: Phys. Metall. Mater. Sci. 35A (4) (2004) 1369–1379.
[8] J.K. Jong, J. Mater. Sci. 39 (2004) 3849–3851.
[9] W.M. Rainforth, J. Mater. Sci. 39 (2004) 6705–6721.
[10] J.J. Kim, J. Mater. Sci. 41 (18) (2006) 6178–6180.
[11] K.C. Goretta, F. Gutierrez-Mora, T. Tran, J. Katz, J.L. Routbort, T.S. Orlova, A.R. de Arellano-Lopez, Ceram. Trans. (2002) 139 (Advances in Ceramic Matrix Composites VIII), 139–146.
[12] F. Toschi, C. Melandri, P. Pinasco, E. Roncari, S. Guicciardi, G. de Portu, J. Am. Ceram. Soc. 86 (9) (2003) 1547–15553.
[13] I. Hussainova, Wear 258 (2005) 357–365.
[14] A.H. Jones, Wear 258 (2005) 942–952.
[15] Z. Liu, Z. Ning, F. Li, X. Yao, S. Ren, J. Mater. Sci. Technol. (Shenyang, China) 21 (5) (2005) 719–723.
[16] R. Rattan, J. Bijwe, Wear 262 (5–6) (2007) 568–574.
[17] I. Finnie, Wear 3 (1960) 87–103.
[18] H. Conrad, D. McCabe, G.A. Sargent, in: R.K. Viswanadham (Ed.), Science of Hard Materials, Plenum Press, New York, 1983, p. 775.
[19] K. Anand, H. Conrad, Mater. Sci. Eng. A 105/106 (1988) 411–421.
[20] S.K. Hovis, J.E. Talia, R.O. Scattergood, Wear 108 (1986) 139–155.
[21] J.L. Ortiz-Merino, R. Todd, Acta Mater. (2005) 3345–3357.
[22] J.A. Hawk, D.E. Alman, Wear 225–229 (1999) 544–556.
[23] A.H. Jones, R.S. Dobedoe, M.H. Lewis, J. Eur. Ceram. Soc. 21 (2000) 969–980.
[24] J. Hu, D.Y. Li, R. Llewellyn, Wear 259 (2005) 6–17.
[25] B.A. Cook, J.L. Harringa, T.L. Lewis, A.M. Russell, Scr. Mater. 42 (2000) 597–602.
[26] B.A. Cook, J.L. Harringa, T.L. Lewis, A.M. Russell, Y. Lee, J. Adv. Mater. 36 (2004) 56–63.
[27] B.A. Cook, J.L. Harringa, A.M. Russell, S.A. Batzer, J. Mach. Sci. Technol. 7 (1) (2003) 157–165.
[28] V. Bedekar, D. Bhat, S. Batzer, L. Walker, Chemical interdiffusion study of ultra-hard ceramic AlMgB14 in the machining of aerospace alloys, Presented at the Great Southwest International Region X Graduate Student Technical Conference (GSTC), Houston, Texas, March 28–29, 2003.
[29] Y. Tian, A.F. Bastawros, C.C.H. Lo, A.P. Constant, A.M. Russell, B.A. Cook, Appl. Phys. Lett. 83 (2003) 1–4.
[30] Y. Tian, G. Li, N.L. Wang, B.A. Cook, A.P. Constant, A.M. Russell, J.E. Snyder, Appl. Phys. Lett. 85 (2004) 967.
[31] A. Ahmed, S. Bahadur, B.A. Cook, J. Peters, Tribol. Int. 39 (2006) 129–137.
[32] J. Peters, B.A. Cook, J.L. Harringa, A.M. Russell, Adv. Powder Metall. Partic. Mater. (2003) 205–215 (Metal Powder Industries Federation, ISSN: 1065-5824).
[33] B. Latella, B.H. O'Connor, J. Am. Ceram. Soc. 82 (1999) 2145–2149.
[34] T.L. Lewis, A.M. Russell, B.A. Cook, J.L. Harringa, Mater. Sci. Eng. A 351 (2003) 117–122.
[35] B. Lawn, Fracture of Brittle Solids, 2nd ed., Cambridge Solid State Science Series, Cambridge University Press, Cambridge, 1993.
[36] B.R. Lawn, J. Mater. Res. 19 (2004) 22–29.
[37] T. Quadir, P.G. Shewmon, Metall. Trans. 12A (1981) 1163–1176.
[38] B.R. Lawn, B.J. Hockey, S.M. Wiederhorn, J. Am. Ceram. Soc. (1980) 356–358.
[39] B.A. Latella, B.H. O'Connor, J. Mater. Sci. (2000) 3505–3517.
[40] A. Warren, A. Nylund, I. Olefjord, Int. J. Refract. Met. Hard Mater. 14 (5–6) (1996) 345.
[41] W. Acchar, U. Gomes, W. Kaysser, J. Goring, Mater. Charact. 43 (1) (1999) 27.
[42] B.A. Cook, A.M. Russell, J.S. Peters, J.L. Harringa, J. Phys. Chem. Solids 71 (2010) 824–826.
[43] S. Li, R.J. Arsenault, P. Jena, J. Appl. Phys. 64 (1988) 6246.
[44] J.S. Peters, B.A. Cook, J.L. Harringa, A.M. Russell, Wear 266 (2009) 1171–1177.
[45] H. Holleck, H. Leiste, W. Schneider, Int. J. Refract. Hard Met. 6 (1987) 149–154.
[46] D. Brodkin, A. Zavaliangos, S.R. Kalidindi, M.W. Barsoum, J. Am. Ceram. Soc. 82 (3) (1999) 665–672.
[47] M. Gu, C. Huang, B. Zou, B. Liu, Mater. Sci. Eng. A 433 (2006) 39–44.
[48] C. Higdon, B. Cook, J. Harringa, A. Russell, J. Goldsmith, J. Qu, P. Blau, Friction and wear mechanisms in AlMgB14-TiB2 nanocoatings," presented at the 18th Wear of Materials conference, Philadelphia, PA April 3–7, 2011.